NANO LETTERS

2008
Vol. 8, No. 6
1619-1624

Ultrafast Electron and Hole Dynamics in Germanium Nanowires

R. P. Prasankumar,* S. Choi, S. A. Trugman, S. T. Picraux, and A. J. Taylor

Center for Integrated Nanotechnologies, Los Alamos National Laboratory, Los Alamos, New Mexico 87545

Received January 21, 2008; Revised Manuscript Received April 7, 2008

ABSTRACT

We present the first ultrafast time-resolved optical measurements, to the best of our knowledge, on ensembles of germanium nanowires. Vertically aligned germanium nanowires with mean diameters of 18 and 30 nm are grown on (111) silicon substrates through chemical vapor deposition. We optically inject electron−hole pairs into the nanowires and exploit the indirect band structure of germanium to separately probe electron and hole dynamics with femtosecond time resolution. We find that the lifetime of both electrons and holes decreases with decreasing nanowire diameter, demonstrating that surface effects dominate carrier relaxation in semiconductor nanowires.

Current research in nanoscience has focused on understanding and controlling nanoscale phenomena in semiconductors, primarily due to the considerable potential of quantum semiconductor devices in real world applications. Much effort has thus been devoted in recent years to an extensive characterization of the size-dependent changes in semiconductor properties when confined in one or more dimensions to nanometer size scales, enabling researchers to rationally design the properties of semiconductor nanostructures for a given application in a manner not afforded by bulk materials. The vast majority of these efforts focused on designing, fabricating, and characterizing two-dimensional (quantum well) and zero-dimensional (quantum dot) nanostructures and devices. However, surprisingly little attention was given to the study of one-dimensional nanostructures, primarily because of challenges in their growth and fabrication. This emphasis has drastically changed in recent years as bottom-up growth techniques have matured, enabling the fabrication of high quality semiconductor nanowires (NWs) and nanowire-based devices. Therefore, efforts aimed at uncovering the novel electronic and optical properties exhibited by semiconductor NWs and exploring their potential for applications in a variety of areas such as chemical and biological sensing, thermoelectrics, nanoelectronics, and nanophotonics are of widespread interest.[1–5]

Arguably, the most promising application of semiconductor NWs is in the area of nanophotonics, where they can serve as multifunctional building blocks in the drive to integrate photonic and electronic devices on a single chip. Nanowire-based lasers, photodetectors, light-emitting diodes (LEDs), waveguides, frequency converters, and transistors have recently been demonstrated,[6] utilizing the unique optical and electronic properties of semiconductor NWs to deliver enhanced functionality. However, an understanding of non-equilibrium carrier dynamics in these nanostructures on a femtosecond time scale will be critical to the design and optimization of NW-based optical devices, particularly as NWs are assembled into more complex arrangements to create nanophotonic devices with advanced functionality.

Ultrafast optical spectroscopy is the only method capable of measuring quasiparticle dynamics as a function of parameters including photon energy, incident fluence, and temperature with femtosecond time resolution. Although a multitude of ultrafast spectroscopic studies have been performed on semiconductor quantum wells (QW),[7] quantum dots (QD),[8] and combinations thereof,[9] relatively few optical measurements with subpicosecond time resolution have been performed on semiconductor nanowires.[6,10–16] In fact, optical pump−probe spectroscopy, arguably the simplest ultrafast optical measurement, has not been applied to the study of dynamics in free-standing, vertically aligned nanowires, to the best of our knowledge. This technique probes the sum of electron and hole distributions at a given photon energy and therefore has the potential to separately measure electron and hole dynamics in semiconductor nanostructures. This method contrasts with time-resolved photoluminescence (TRPL) measurements, which measure the product of electron and hole distributions and therefore cannot separately probe electron and hole dynamics.[8] Therefore, it can be expected that optical pump−probe measurements on semiconductor nanowires may reveal physics unique to the one-dimensional nature of these nanoscale structures, while enabling the measurement of parameters important for nanophotonic applications of NW-based devices.

* Corresponding author. E-mail: rpprasan@lanl.gov.

10.1021/nl080202+ CCC: $40.75
Published on Web 05/07/2008

In this work, we present the first ultrafast optical measurements on free-standing, vertically aligned semiconductor NWs. Germanium was the material of choice because of our ability to grow high quality, vertically aligned NW ensembles on silicon (111) substrates;[17] its relevance to many photonic, electronic, and thermoelectric applications also makes it particularly worth investigating.[17,18] In addition, the indirect band gap in Ge allows us to independently measure electron and hole dynamics after femtosecond optical excitation in bulk Ge and Ge NWs by simply tuning the probe wavelength. We can therefore optically inject carriers and separately track the temporal evolution of electron and hole populations in the NWs. Measurements on 18 and 30 nm diameter NWs reveal that electrons and holes are trapped in fast surface states within ~16 ps, with the lifetime strongly depending on NW diameter for both carrier species. The electron and hole diffusion lengths and surface recombination velocities can also be extracted from these ultrafast measurements, underlining the ability of ultrafast optical spectroscopy to measure parameters central to the operation of NW-based devices. Our experiments clearly demonstrate the dominance of surface trapping and nonradiative recombination processes over carrier relaxation in semiconductor NWs.

The growth of our Ge NW samples has previously been described in ref 17 and will only be briefly described here. Gold nanoparticles were self-assembled through thermal evaporation of 2 and 4 nm thick Au on hydrogen terminated clean Si(111) substrates and used as catalytic seeds for subsequent Ge NW growth. Single crystal nanowires were then grown in a low pressure chemical vapor deposition (CVD) chamber by exposing the substrates to germane in a hydrogen carrier gas. Growth was carried out at a germane partial pressure of 780 mT in a two-step temperature process (420 °C for 2 min followed by 375 °C for 7 min). Scanning electron microscopy (SEM) and transmission electron microscopy (TEM) were used to characterize the crystal structure, growth direction, epitaxial relationship to the Si substrate, diameter, and length of the NWs. The Ge NWs were found to be single crystalline and epitaxial with respect to the Si substrate, with growth primarily along the <111> direction. Two samples were synthesized using the above two Au seed conditions with average NW lengths of 1.6 μm and average diameters of $d = 18$ and 30 nm (Figure 1, inset), respectively. SEM images (Figure 1) reveal that NWs in both samples exhibit a high degree of vertical alignment, with a nearly constant diameter along the full length of the NW. No significant growth of uncatalyzed Ge was observed in these samples. The areal densities of the NWs were approximately 157 NW/μm^2 and 119 NW/μm^2 for the 18 and 30 nm diameter NWs, respectively.

Optical pump−probe experiments were based on a 100 kHz regeneratively amplified Ti:sapphire laser system producing 50 fs, 10 μJ pulses at 800 nm. The output beam is split into two equal parts to concurrently pump two optical parametric amplifiers (OPA). The visible OPA produces a signal beam tunable from 480−700 nm, an idler beam tunable from 930−2300 nm, and a residual pump beam at 400 nm. Similarly, the IR OPA produces a signal tunable

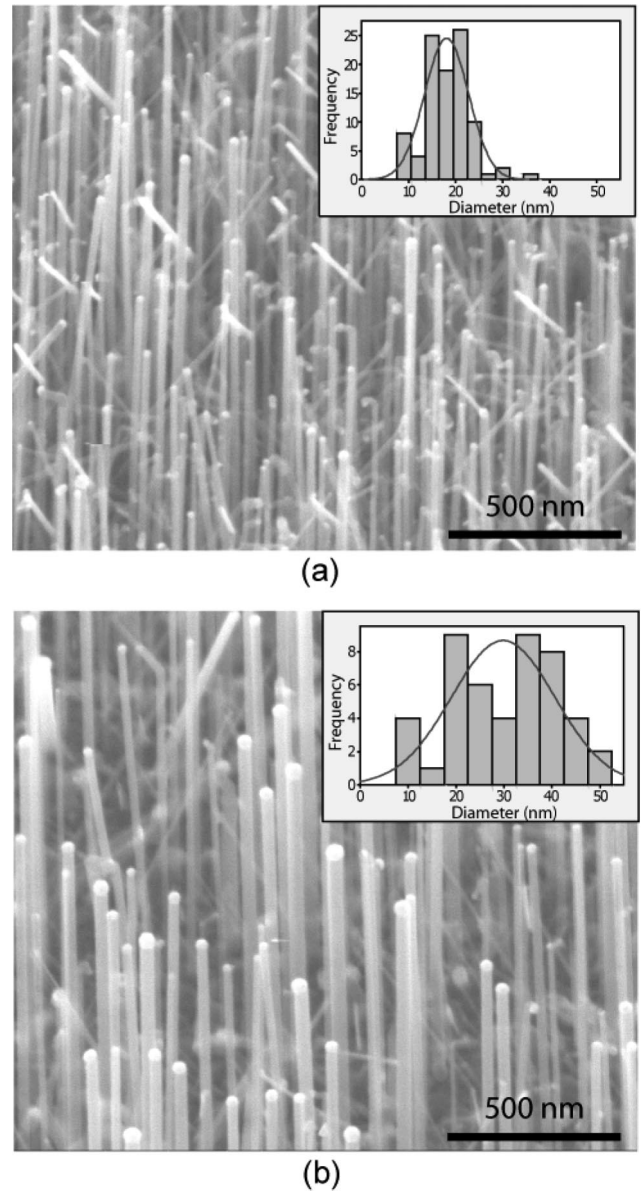

Figure 1. SEM images, taken at a 45° tilt angle, of vertically aligned Ge NWs with average diameters of (a) 18 nm and (b) 30 nm. The insets show representative histograms of the NW size distributions.

from 1.1−1.6 μm and an idler tunable from 1.6−2.4 μm, with a residual pump at 800 nm. This setup enables measurements with independently tunable pump and probe wavelengths over a range of 400 nm (3.1 eV) to 3 μm (0.41 eV) and sub-100 fs time resolution. In the experiments described here, the pump wavelength was 800 nm (1.55 eV), and the pulse duration was ~60 fs, while the probe wavelengths were 550 nm (2.25 eV) and 1200 nm (1.03 eV), with pulse durations of ~31 fs. The pump pulse creates electron−hole pairs (ehp) at the direct bandgap in Ge (~0.8 eV) with a carrier density of $\sim 2 \times 10^{19}$ cm^{-3} (fluence ~81 μJ/cm^2). This corresponds to a density of $\sim 5 \times 10^3$ ehp/NW and $\sim 10^4$ ehp/NW in the 18 and 30 nm diameter NWs, respectively. All measurements were performed at room temperature with the probe near normal incidence and the pump at a 45° incidence angle; both beams were *s* polarized,

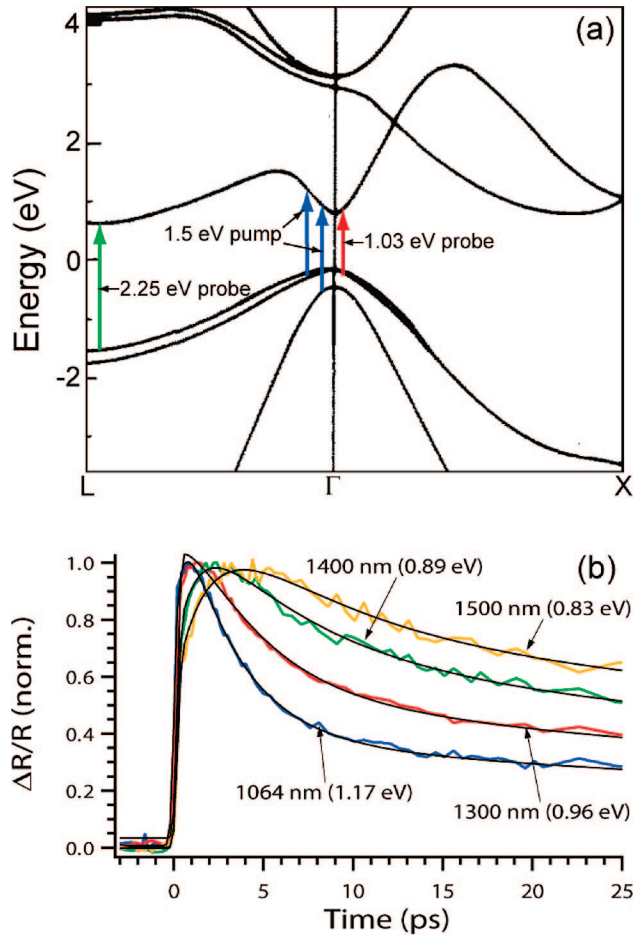

Figure 2. (a) Schematic bandstructure of Ge (as in ref 24), with optical transitions indicated on the figure. (b) Optical pump, near-IR probe measurements on bulk Ge, with the probe wavelength indicated for each trace.

perpendicular to the NW axis. Finally, it is important to note that although the radii of the NWs studied here are comparable to the exciton Bohr radius (~24 nm) in Ge,[19] several calculations[20,21] and experiments[22,23] have indicated that quantum effects should be negligible for NW diameters >10 nm, allowing us to utilize the band structure of bulk Ge in interpreting our data.

The band structure of bulk Ge is depicted in Figure 2a,[24] including allowed optical transitions for the pump and probe pulses. Previous theoretical calculations of femtosecond differential transmission in bulk Ge demonstrated that the majority of electrons rapidly scatter to the X valley and subsequently to the L valley (within ~4 ps) following above band gap photoexcitation at the Γ point.[25] Holes optically excited in the split off and light hole bands also scatter to the heavy hole band on a ~1 ps time scale. Therefore, after the first few picoseconds, a hot distribution of electrons exists at the L valley minimum, with a corresponding distribution of holes at the Γ point.[26] Previous differential reflectivity measurements with degenerate 800 nm pump and probe pulses supported this hypothesis and demonstrated that hole dynamics can be independently measured with near-IR probe pulses.[27] In addition, the presence of a nonequilibrium electron distribution in the L valley suggests that visible (450−600 nm) probe pulses can monitor the temporal evolution of this population because of the large joint density of states for optical transitions in this wavelength range; this has been previously demonstrated for Ge nanoparticles.[23] Therefore, upon optical excitation at 800 nm, the temporal evolution of electron and hole populations in Ge after the first few picoseconds can be probed by visible and near-IR probe pulses, respectively, allowing us to independently measure electron and hole dynamics. By assuming that quantum effects can be neglected for NWs with $d > 10$ nm, it follows that we can similarly isolate electron and hole dynamics in Ge NWs by tuning the probe wavelength.

To verify this concept and compare it with the theoretical calculations in ref 25, we performed optical-pump, near-IR probe measurements on bulk Ge in reflection at near normal incidence (Figure 2b); the data is normalized to facilitate comparison of the rise and fall times of the $\Delta R/R$ signals. It is worth noting that the $\Delta R/R$ signal was negative at all wavelengths, with the magnitude increasing with wavelength, as expected from ref 25. The rise of the $\Delta R/R$ signal is due to hole relaxation from their initially photoexcited states high above the band gap into lower energy states that are probed by the near-IR pulse, while the decrease in the signal is due to the relaxation of holes out of these states toward the valence band maximum. It is clear from this figure that the rise (~0.5−2 ps) and fall (~55−120 ps) times of the differential reflectivity signal increase with probe wavelength, as expected. This data agrees well with the calculated traces in ref 25, further supporting the ability of our near-IR probe pulses to isolate hole dynamics with femtosecond time resolution. Similar experiments were performed on bulk Ge with visible (500−650 nm) probe pulses (not shown); the measured electron dynamics varied little with wavelength, as the joint density of states is nearly constant with energy in this range.

Optical-pump, visible/near-IR probe experiments were then performed on the two Ge NW samples to examine electron and hole relaxation in these systems. Figure 3 depicts measurements of (a) electron and (b) hole dynamics in the $d = 18$ and $d = 30$ nm NW ensembles, with the corresponding $\Delta R/R$ signals from bulk Ge shown for comparison. The peak amplitudes of all traces in Figure 3a,b were normalized to facilitate comparison of carrier lifetimes; the measured $\Delta R/R$ signals from the Ge NWs (before normalizing) were positive, with the signal from bulk Ge negative as described above. This can be understood by considering that the NWs occupy <9% of the total surface area and therefore minimally reflect the pump and probe light, with the bulk of the reflection actually occurring at the Si substrate. Therefore, the NWs are effectively measured in transmission ($\Delta R/R \approx \Delta T/T$), which results in a positive signal due to absorption saturation in the NWs. To verify that the measured $\Delta R/R$ signals were not significantly influenced by carrier dynamics in the substrate, we also performed experiments on Si substrates coated with seed Au nanoparticles before NW growth. The observed signals were more than an order of magnitude smaller than those from the NW samples,

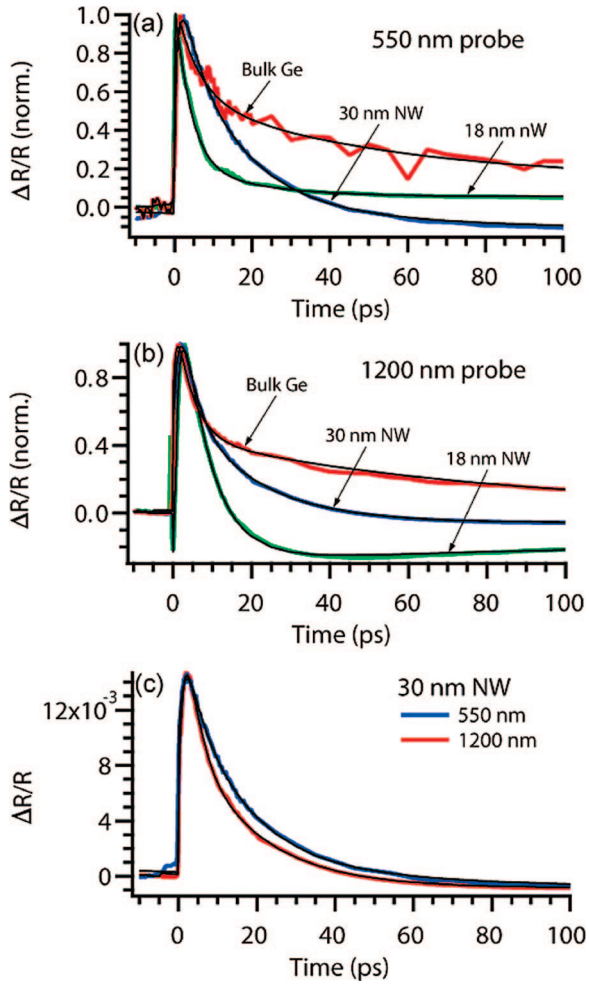

Figure 3. Optical pump−probe measurements on Ge NWs. The pump wavelength was 800 nm (1.55 eV), and the probe wavelength was set to (a) 550 nm (2.25 eV) and (b) 1200 nm (1.03 eV) to probe electron and hole dynamics, respectively. (c) Comparison of electron and hole dynamics for 30 nm NWs. This data is not normalized, clearly showing the correspondence between electron and hole dynamics in this sample.

demonstrating that the $\Delta R/R$ signals shown in Figure 3 are due to carrier dynamics in the Ge NWs.

Immediately apparent from Figure 3a,b is the rapid decay of the photoexcited electron and hole populations in the NWs, contrasting strongly with the relatively long-lived $\Delta R/R$ signals in bulk Ge. It can also be seen that the carrier lifetime decreases with the NW diameter. This is suggestive of a surface-mediated mechanism, as the large surface-to-volume ratio of these one-dimensional systems makes them more sensitive to surface effects than the bulk material. Several publications have previously indicated that surface trapping and subsequent nonradiative recombination dominate carrier relaxation in semiconductor NWs.[15,18,28–32] In germanium, these surface states have been categorized into two types, "fast" and "slow", with the fast surface states governing carrier recombination on timescales of picoseconds to nanoseconds and the slow surface states influencing carrier transport on timescales of seconds to hundreds of seconds.[18,33] The slow surface states in Ge NWs have been extensively characterized in ref 18, but to the best of our knowledge, the fast surface states that are responsible for nonradiative recombination in Ge NWs have yet to be studied. Ultrafast optical pump−probe spectroscopy is of particular utility in measuring the time scale for carrier trapping by fast surface states in Ge NWs, as the TRPL measurements that have been used to characterize surface recombination in direct band gap semiconductors[28–30] would be difficult because of the rapid separation of the electron and hole populations in momentum space, inhibiting radiative recombination. In fact, the optical pump−probe measurements depicted in Figure 3 allow us to construct a physical picture of carrier dynamics in Ge NWs after ultrafast optical excitation.

Table 1. Comparison of Electron and Hole Lifetimes (τ_e, τ_h), Surface Recombination Velocities (S_e, S_h), and Diffusion Lengths (L_e, L_h) for 18 nm NWs, 30 nm NWs, and Bulk Ge[a]

	18 nm diameter NWs	30 nm diameter NWs	bulk Ge
τ_e (ps)	5.5	15.2	52
τ_h (ps)	7	16.3	59
S_e (cm/s)	9.1×10^4	6.4×10^4	
S_h (cm/s)	7.2×10^4	5.9×10^4	
L_e (nm)	238	396	721
L_h (nm)	194	297	543

[a] The bulk diffusion constants, $D_e = 103$ cm^2/s for electrons and $D_h = 54$ cm^2/s for holes,[26] were used to calculate S_e, S_h, L_e, and L_h.

The pump pulse creates an electron−hole plasma in the Ge NWs at $t = 0$, due to the high density of photoexcited carriers (well above the Mott density of $\sim 10^{17}$ cm^{-3}) that prevent exciton formation through screening.[23,30] Band gap renormalization (BGR) effects have also been shown to affect TRPL experiments at these carrier densities;[29,30] we calculate the BGR to be ~20 meV, which does not significantly influence our data since this is comparable to the bandwidth of our ultrashort pump and probe pulses. As in bulk Ge, the rise times of the $\Delta R/R$ signals at 550 and 1200 nm are due to rapid electron scattering from the Γ point to the L valley and hole scattering from the split off and heavy hole bands to the light hole bands, respectively. Curve fits to the measured data indicate that these processes occur on timescales of ~1.75 ps (electrons) and ~1.35 ps (holes), varying little with NW diameter. The photoexcited electrons and holes then rapidly thermalize through phonon scattering and Auger scattering processes[14,26] on a time scale of a few picoseconds, comparable to that in the bulk material. However, Figure 3a,b clearly shows that after the first few picoseconds, the $\Delta R/R$ signal decays much more rapidly in the NWs than in bulk Ge; in fact, the $\Delta R/R$ signal for the 18 nm NWs at 550 nm immediately starts decreasing after reaching its peak at $t \approx 500$ fs. This can be quantified through curve fits to the traces in Figure 3a,b; the electron and hole lifetimes obtained for the 18 nm NWs, 30 nm NWs, and bulk Ge are given in Table 1. The origin of the rapid decrease in the $\Delta R/R$ signal for the NWs (as compared with bulk Ge) is carrier trapping at the NW surface, qualitatively supported by the observed decrease in carrier lifetimes with decreasing NW diameter. At longer time delays, the $\Delta R/R$ signals for certain traces decrease below zero. This is likely due to induced absorption of the probe photons, promoting carriers trapped at surface states to higher energy states from which they eventually recombine (corresponding to the increase in

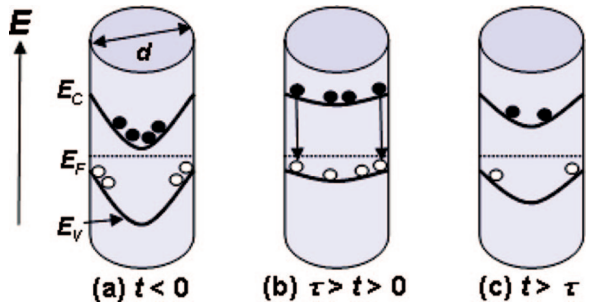

Figure 4. Schematic depicting the influence of NW surface properties on carrier dynamics in Ge NWs: (a) before photoexcitation, (b) at early times, and (c) at long times, after most carriers have recombined.

the $\Delta R/R$ signal for the 18 nm NWs in Figure 3b after ~40 ps). However, further experiments are necessary to verify this. In the remainder of this paper, we focus on the initial rapid decay, into which more insight can be obtained by considering the effects of NW surface properties on optically excited carriers as follows below (Figure 4).

Most semiconductors are known to exhibit a depletion space charge layer near the surface,[34] which in NWs can be on the order of the wire diameter. In intrinsic Ge NWs, this is due to an oxide layer that forms on the surface of untreated NWs, contributing trap levels that are filled with electrons when below the Fermi level; these trap levels are typically ~0.15 eV below the middle of the band gap in Ge.[18] The resulting negative electric field at the surface bends the conduction and valence bands upward in energy, causing holes to accumulate near the surface to maintain charge neutrality. This spatially separates the electron and hole populations in thick NWs, with holes near the surface and electrons accumulating at the center of the NW (Figure 4a).[18,31,35,36] However, it has been shown that, for thin GaN NWs (d < 80 nm), the NW is completely depleted and surface recombination is enhanced relative to thick NWs.[31]

At low photoexcited carrier densities, the built in surface field will cause holes to be rapidly trapped at the surface, while electrons must surmount a potential barrier to reach the surface. One would therefore expect the measured lifetimes for electrons to be longer than those of holes in our experiments. In contrast, it can be seen from Figure 3c and Table 1 that not only the lifetimes but also the magnitude of the $\Delta R/R$ signals for both electrons and holes are nearly identical in the 30 nm NWs. This can be understood by noting that the photoexcited carrier densities in our experiments are high enough to screen the negative surface field, reducing band bending and increasing the probability for both types of carriers to migrate to the surface and nonradiatively recombine at trap states (Figure 4b).[35,36] At later times, after the carrier density has decreased, the negative surface field will be restored, inhibiting electron diffusion to the surface (Figure 4c). This may account for the slight difference in lifetimes for electrons and holes seen in Figure 3c. A more pronounced difference in electron and hole lifetimes would likely be observed for lower photoexcited carrier densities and/or thicker NWs.

The dependence of carrier lifetimes on NW diameter (Table 1) can be more quantitatively understood using a model described in ref 31 to explain the size dependence of the photocurrent in semiconductor NWs. In this model, the carrier lifetime $\tau_{e,h} \sim d^2$ for thin NWs under the assumptions of homogeneous photoexcitation, a lifetime dominated by surface recombination, and a minimal effect of the photoexcited carrier density on the band structure within the NWs. The last assumption is questionable in our experiments because of the high photoexcited carrier densities; however, when applying this model to our data, we find that the ratio of carrier lifetimes, τ (30 nm NW)/τ (18 nm NW) = 2.76 for electrons and 2.33 for holes, comparing well with the ratio of squared NW diameters, (30 nm)^2/(18 nm)^2 = 2.77. This scaling of the carrier lifetimes with NW diameter clearly demonstrates that surface-related phenomena dominate carrier relaxation in Ge NWs.

We can also extract device-relevant parameters such as the electron and hole diffusion lengths and surface recombination velocities from our time-resolved spectroscopic measurements. The electron diffusion length L_e is proportional to, $\sqrt{D_e \tau_e}$, where D_e is the electron diffusion constant; a similar relation holds for the hole diffusion length L_h. Using the bulk values for D_e and D_h,[37] we find that the diffusion lengths, given in Table 1, are roughly 1 order of magnitude greater than the NW diameter, as previously observed in time-resolved PL measurements on InP NWs.[30] This implies that the photoexcited carriers scatter off the NW walls several times before recombining.

Finally, we can calculate the surface recombination velocity, S, for electrons and holes in these Ge NWs to quantify the influence of surface effects and compare to previous measurements on NWs with different compositions. Here, we use a model given in ref 37 to calculate the surface recombination velocity for cylindrically shaped NWs, with the results given in Table 1. We find $S \sim 7 \times 10^4$ cm/s, on average, for electrons and holes in our NWs. This is larger than surface recombination velocities measured in InP NWs (~600−4000 cm/s)[29,30] using time-resolved PL but smaller than those measured in GaAs NWs (>10^6 cm/s).[15] The surface recombination velocities measured here with optical pump−probe spectroscopy compare reasonably well to surface recombination velocities measured in Si NWs ($S \sim 3 \times 10^5$ cm/s) using electron-beam-induced current (EBIC) microscopy.[37] The similarity of these values of S, measured on group IV NWs by entirely different experimental techniques, further demonstrates the viability of ultrafast optical spectroscopy for characterizing fundamental NW properties. The relatively high values of S measured here can be attributed to the untreated NW surface; we expect that surface passivation through chemical treatment or growth of a semiconductor shell will significantly increase carrier lifetimes and reduce surface recombination velocities, making these one-dimensional systems more useful for various optical and electronic applications.

In conclusion, we have used ultrafast optical pump−probe spectroscopy to independently measure electron and hole dynamics in free-standing, vertically aligned Ge nanowires

for the first time. We find that the carrier lifetime is ≤16 ps, scaling with the NW diameter in accordance with a model based on carrier recombination at the NW surface. In addition, we observe that the lifetimes of electrons and holes are comparable at the investigated carrier densities because of screening of the built in surface electric field by the photoexcited carriers. Finally, we are able to extract the surface recombination velocity and diffusion lengths for both electrons and holes in Ge NWs from our measurements, parameters relevant to future incorporation of these NWs into thermoelectric, nanoelectronic, and nanophotonic devices. These experiments are only the first steps in using ultrafast optical spectroscopy to explore carrier dynamics in semiconductor NWs; future experiments are expected to give further insight into the physics of these fascinating nanosystems, allowing researchers to optimize them for a variety of applications.

Acknowledgment. This work was performed at the Center for Integrated Nanotechnologies, a U.S. Department of Energy, Office of Basic Energy Sciences user facility and also partially supported by the NNSA's Laboratory Directed Research and Development Program. Los Alamos National Laboratory, an affirmative action equal opportunity employer, is operated by Los Alamos National Security, LLC, for the National Nuclear Security Administration of the U.S. Department of Energy under Contract No. DE-AC52−06NA25396.

References

(1) Agarwal, R.; Lieber, C. M. *Appl. Phys. A: Mater. Sci. Process.* **2006**, *85*, 209.
(2) Law, M.; Goldberger, J.; Yang, P. *Annu. Rev. Mater. Res.* **2004**, *34*, 83.
(3) Li, Y.; Qian, F.; Xiang, J.; Lieber, C. M. *Materials Today* **2006**, *9*, 18.
(4) Thelander, C.; Agarwal, P.; Brongersma, S.; Eymery, J.; Feiner, L. F.; Forchel, A.; Scheffler, M.; Riess, W.; Ohlsson, B. J.; Gosele, U.; Samuelson, L. *Materials Today* **2006**, *9*, 28.
(5) Pauzauskie, P. J.; Yang, P. *Materials Today* **2006**, *9*, 36.
(6) Sirbuly, D. J.; Law, M.; Yan, H.; Yang, P. *J. Phys. Chem. B* **2005**, *109*, 15190.
(7) Shah, J. *Ultrafast spectroscopy of semiconductors and semiconductor nanostructures*; Springer: New York, 1999.
(8) Norris, T. B.; Kim, K.; Urayama, J.; Wu, Z. K.; Singh, J.; Bhattacharya, P. *J. Phys. D: Appl. Phys* **2005**, *38*, 2077.
(9) Prasankumar, R. P.; Attaluri, R. S.; Averitt, R. D.; Urayama, J.; Weisse-Bernstein, N.; Rotella, P.; Stintz, A.; Krishna, S.; Taylor, A. J. *Opt. Express* **2008**, *16*, 1165.
(10) Johnson, J. C.; Knutsen, K. P.; Yan, H.; Law, M.; Zhang, Y.; Yang, P.; Saykally, R. J. *Nano Lett.* **2004**, *4*, 197.
(11) Song, J. K.; Szarko, J. M.; Leone, S. R.; Li, S.; Zhao, Y. *J. Phys. Chem. B* **2005**, *109*, 15749.
(12) Sun, C.-K.; Sun, S.-Z.; Lin, K.-H.; Zhang, K. Y.-J.; Liu, H.-L.; Liu, S.-C.; Wu, J.-J. *Appl. Phys. Lett.* **2005**, *87*, 023106.
(13) Baxter, J. B.; Schmuttenmaer, C. A. *J. Phys. Chem. B* **2006**, *110*, 25229.
(14) Robel, I.; Bunker, B. A.; Kamat, P. V.; Kuno, M. *Nano Lett.* **2006**, *6*, 1344.
(15) Parkinson, P.; Lloyd-Hughes, J.; Gao, Q.; Tan, H. H.; Jagadish, C.; Johnston, M. B.; Herz, L. M. *Nano Lett.* **2007**, *7*, 2162.
(16) Othonos, A.; Lioudakis, E.; Philipose, U.; Ruda, H. E. *Appl. Phys. Lett.* **2007**, *91*, 241113.
(17) Dailey, J. W.; Taraci, J.; Clement, T.; Smith, D. J.; Drucker, J.; Picraux, S. T. *J. Appl. Phys.* **2004**, *96*, 7556.
(18) Hanrath, T.; Korgel, B. A. *J. Phys. Chem. B* **2005**, *109*, 5518.
(19) Maeda, Y. *Phys. Rev. B* **1995**, *51*, 1658.
(20) Kholod, A. N.; Shaposhnikov, V. L.; Sobolev, N.; Borisenko, V. E.; D'Avitaya, F. A.; Ossicini, S. *Phys. Rev. B* **2004**, *70*, 035317.
(21) Harris, C.; O'Reilly, E. P. *Physica E* **2006**, *32*, 341.
(22) Haight, R.; Sirinakis, G.; Reuter, M. *Appl. Phys. Lett.* **2007**, *91*, 233116.
(23) Stagira, S.; Nisoli, M.; De Silvestri, S.; Tognini, P.; Stella, A.; Cheyssac, P.; Kofman, R. *Phys. Rev. B* **2000**, *62*, 10318.
(24) Chelikowsky, J. R.; Cohen, M. L. *Phys. Rev. B* **1976**, *14*, 556.
(25) Bailey, D. W.; Stanton, C. J. *J. Appl. Phys.* **1995**, *77*, 2107.
(26) Othonos, A. *J. Appl. Phys.* **1998**, *83*, 1789.
(27) Zollner, S.; Myers, K. D.; Jensen, K. G.; Dolan, J. M.; Bailey, D. W.; Stanton, C. J. *Solid State Commun.* **1997**, *104*, 51.
(28) Titova, L. V.; Hoang, T. B.; Jackson, H. E.; Smith, D. C.; Yarrison-Rice, J. M.; Lensch, J. L.; Lauhon, L. J. *Appl. Phys. Lett.* **2006**, *89*, 053119.
(29) Reitzenstein, S.; Munch, S.; Hofmann, C.; Forchel, A.; Crankshaw, S.; Chuang, L. C.; Moewe, M.; Chang-Hasnain, C. *Appl. Phys. Lett.* **2007**, *91*, 091103.
(30) Titova, L. V.; Hoang, T. B.; Yarrison-Rice, J. M.; Jackson, H. E.; Kim, Y.; Joyce, H. J.; Gao, Q.; Tan, H. H.; Jagadish, C.; Zhang, X.; Zou, J.; Smith, L. M. *Nano Lett.* **2007**, *7*, 3383.
(31) Calarco, R.; Marso, M.; Richter, T.; Aykanat, A. I.; Meijers, R.; Hart, A. v. d.; Stoica, T.; Luth, H. *Nano Lett.* **2005**, *5*, 981.
(32) Chin, A. H.; Ahn, T. S.; Li, H.; Vaddiraju, S.; Bardeen, C. J.; Ning, C.-Z.; Sunkara, M. K. *Nano Lett.* **2007**, *7*, 626.
(33) Bardeen, J.; Coovert, R. E.; Morrison, S. R.; Schrieffer, J. R.; Sun, R. *Phys. Rev.* **1956**, *104*, 47.
(34) Bardeen, J. *Phys. Rev.* **1947**, *71*, 717.
(35) Mattila, M.; Hakkarainen, T.; Lipsanen, H.; Jiang, H.; Kauppinen, E. I. *Appl. Phys. Lett.* **2007**, *90*, 033101.
(36) van Weert, M. H.M.; Wunnicke, O.; Roest, A. L.; Eijkemans, T. J.; Silov, A. Y.; Haverkort, J. E. M.; 't Hooft, G. W.; Bakkers, E. P. A. M. *Appl. Phys. Lett.* **2006**, *88*, 043109.
(37) Allen, J. E.; Hernesath, E. R.; Perea, D. E.; Lensch-Falk, J. L.; Li, Z. Y.; Yin, F.; Gass, M. H.; Wang, P.; Bleloch, A. L.; Palmer, R. E.; Lauhon, L. J. *Nat. Nanotechnol.* **2008**, *3*, 168.

NL080202+